



# Design, synthesis and molecular docking studies of thymol based 1,2,3-triazole hybrids as thymidylate synthase inhibitors and apoptosis inducers against breast cancer cells

Mohammad Mahboob Alam<sup>a</sup>, Azizah M. Malebari<sup>b</sup>, Syed Nazreen<sup>a,\*</sup>, Thikryat Neamatallah<sup>c</sup>, Abdurraheem S.A. Almalki<sup>d,\*</sup>, Ahmed A. Elhenawy<sup>a,e</sup>, Rami J. Obaid<sup>f</sup>, Meshari A. Alsharif<sup>f,g</sup>

<sup>a</sup> Department of Chemistry, Faculty of Science, Albaha University, Albaha, Saudi Arabia

<sup>b</sup> Department of Pharmaceutical Chemistry, Faculty of Pharmacy, King Abdulaziz University, Jeddah, Saudi Arabia

<sup>c</sup> Department of Pharmacology and Toxicology, Faculty of Pharmacy, King Abdulaziz University, Jeddah, Saudi Arabia

<sup>d</sup> Department of Chemistry, Faculty of Science, Taif University, Taif, Saudi Arabia

<sup>e</sup> Chemistry Department, Faculty of Science, Al-Azhar University, 11884 Nasr City, Cairo, Egypt

<sup>f</sup> Chemistry Department, Faculty of Applied Sciences, Umm Al-Qura University, Makkah, Saudi Arabia

<sup>g</sup> Department of Chemistry, Faculty of Science, University of Tabuk, Tabuk, Saudi Arabia

## ARTICLE INFO

### Keywords:

Thymol  
1,2,3-triazole  
Cell cycle arrest  
Apoptosis  
Thymidylate synthase  
Molecular docking  
DFT

## ABSTRACT

Natural product produced by plants has been the backbone for numerous anticancer agents. In the present work, natural bioactive thymol based 1,2,3-triazole hybrids have been synthesized and evaluated for anticancer activity in MCF-7 and MDA-MB-231 cancer cells. The synthesized molecules displayed desired pharmacokinetic predictions for an orally available drug. Among the synthesized hybrids, compound 4-((2-isopropyl-5-methylphenoxy)methyl)-1-o-tolyl-1H-1,2,3-triazole (**10**) was the most potent (IC<sub>50</sub> 6.17 μM) showing comparable cytotoxicity to tamoxifen (IC<sub>50</sub> 5.62 μM) and 3.2 fold inhibition to 5-fluorouracil (IC<sub>50</sub> 20.09 μM) against MCF-7 cancer cells. Whereas against MDA-MB-231 cancer cells, compound **10** (IC<sub>50</sub> 10.52 μM) and 3-(4-((2-isopropyl-5-methylphenoxy)methyl)-1H-1,2,3-triazol-1-yl)benzoic acid (**12**) (IC<sub>50</sub> 11.41 μM) displayed 1.42 and 1.3 fold inhibition, respectively to tamoxifen (IC<sub>50</sub> 15.01 μM) whereas 2.4 fold and 2.2 activity to 5-Fluorouracil (IC<sub>50</sub> 25.31 μM). Furthermore, **10** and **12** significantly inhibited thymidylate synthase enzyme with 2.4 and 1.26 fold activity to standard drug, Pemetrexed (IC<sub>50</sub> 5.39 μM) suggesting their mode of action as thymidylate synthase inhibitors. Cell cycle arrest and annexin V induced apoptosis study of compound **10** showed cell cycle arrest at the G2/M phase and induction of apoptosis in MCF-7 cells. The molecular docking was accomplished onto thymidylate synthase (TS) protein. The active compounds exhibited promising binding interactions and binding affinities into active sites. Finally, density functional theory (DFT) calculations including chemical reactivity and molecular electrostatic potential (MEP) have been performed to confirm the data obtained from docking and biological experiments. The results from this study inferred that compound **10** could be served as a lead molecule for the treatment of breast cancer.

## 1. Introduction

Natural product produced by plants has been the backbone for numerous anticancer agents due to wide structural diversity and bioactivity potential.<sup>1,2</sup> Since time immemorial, plants have provided important anticancer leads such as Podophyllotoxins, camptothecin, vinblastine, or paclitaxel which are found to possess excellent antineoplastic potential.<sup>3-5</sup> The molecular modifications of functional groups of

these leads by semisynthesis process have led to the structural analogues with greater pharmacological potential with lesser side effects.<sup>6,7</sup> For example, Etoposide, teniposide, and etopophos are the semisynthetic derivatives of Podophyllotoxin and act as topoisomerase II inhibitors,<sup>8,9</sup> Topotecan and irinotecan as topoisomerase I inhibitors, are derived by modifications of Camptothecin<sup>10-12</sup> whereas Docetaxel, a semisynthetic analogue of Paclitaxel, acts as a microtubulin inhibitor.<sup>13</sup> Some of the semisynthetic derivatives of natural products such as gimatecan,

\* Corresponding authors.

E-mail addresses: [syed.nazreen22885@gmail.com](mailto:syed.nazreen22885@gmail.com), [syed.nazreen@gmail.com](mailto:syed.nazreen@gmail.com) (N. Syed), [drasaalmalki@gmail.com](mailto:drasaalmalki@gmail.com) (A.S.A. Almalki).

<https://doi.org/10.1016/j.bmc.2021.116136>

Received 25 December 2020; Received in revised form 18 March 2021; Accepted 23 March 2021

Available online 20 April 2021

0968-0896/© 2021 Elsevier Ltd. All rights reserved.

fosbratabulin, alvocidib, phenoxodiol are in different clinical trials<sup>14,15</sup> while plant based lead molecules such as curcumin, ingenol mebutate, betulinic acid are in clinical trials for cancer treatment.<sup>16,17</sup>

Thymol, chemically known as 2-isopropyl-5-methylphenol, is a white crystalline monoterpenoid occur mainly in *Thymus vulgaris* (Ajwain), and other plant species. Thymol has emerged as an interesting scaffold in medicinal chemistry due to the various pharmacological activities exhibited by this natural product and its derivatives.<sup>18</sup> Thymol has been reported with antioxidant,<sup>19</sup> antiinflammatory,<sup>20</sup> antimicrobial<sup>21</sup> anticholinesterase<sup>22</sup> and anticancer activities.<sup>23</sup> Thymol has been reported to exert anticancer effect by suppression of cell growth, induction of apoptosis as well as activation of Bcl-2/Bax protein, an apoptosis regulator.<sup>24</sup> On the other hand, 1,2,3-triazole has played a commendable role in drug discovery as they are found to possess anticancer,<sup>25</sup> antimicrobial,<sup>26</sup> anti-inflammatory<sup>27</sup> and antitubercular.<sup>27</sup> 1,2,3-triazole derivatives have shown to exert anticancer effect by inhibition of thymidylate synthase enzyme.<sup>28–30</sup> Thymidylate synthase catalyses deoxythymidine monophosphate (dTMP) formation from deoxyuridine monophosphate (dUMP) which upon phosphorylation leads to dTTP, a precursor for DNA synthesis.<sup>31</sup> Blocking of dTTP subsequently leads to DNA damage causing cell cycle arrests and induction of apoptosis.<sup>32</sup>

In view of the anticancer potential of thymol and 1,2,3-triazoles (Fig. 1), we aim to conjugate both thymol and 1,2,3-triazole moieties under one construct via oxymethylene linker and screened for cytotoxicity against MCF-7 and MDA-MB-231 breast cancer cells. The most active compounds were further tested for *in vitro* thymidylate synthase inhibition, cell cycle arrest and apoptosis studies. The molecular docking combined with density functional theory (DFT) based on chemical reactivity and molecular electrostatic potential (MEP) calculations were carried out to confirm the findings of our biological activities results.

## 2. Results and discussion

### 2.1. Chemistry

The synthetic path of thymol linked 1,2,3-triazole hybrids 3–13 is

summarized in scheme 1. Firstly, propargylation of thymol 1 was carried out using propargyl bromide in presence of dry acetone and anhydrous  $K_2CO_3$  to give propargylated thymol 2. Then, compound 2 was reacted with different aromatic azides using Click chemistry approach to afford thymol linked 1,2,3-triazole hybrids, 3–13. The structures of compound 2–13 were established by using different spectroscopic techniques. The formation of compound 2 was supported from IR spectrum, revealing absorption band at  $3291\text{ cm}^{-1}$  for terminal hydrogen of alkyne group as well as absence of absorption band of hydroxyl group at  $3162\text{ cm}^{-1}$  of thymol. Finally electron spray ionization spectrum of compound 2 displayed molecular ion signal at 189 confirmed its formation. The  $^1\text{H NMR}$  of final compound 3–13 showed a singlet in the range  $\delta$  8.09–8.74 ppm assigned to proton of 1,2,3-triazole ring and absence of acetylenic proton in IR spectrum indicating the acetylenic proton is converted into 1,2,3-triazolic proton, O-CH<sub>2</sub> singlet in the range  $\delta$  5.19–5.43 ppm; aromatic protons in the range  $\delta$  6.74–8.45 ppm and methyl protons in the range  $\delta$  1.24–2.49 ppm. The confirmatory evidence of 1,2,3-triazole ring was also obtained from the  $^{13}\text{C NMR}$  which displayed signal in the range  $\delta$  136.55–136.72 ppm. All the structures were finally confirmed from ESI MS displaying desired molecular ion peak.

### 2.2. In silico ADME/pharmacokinetics studies

The *in silico* ADME properties of the drugs is very important in drug discovery as the pharmacological and pharmacokinetic properties of the molecule must reach the action point in a timely manner, in sufficient concentration and can be eliminated from the body after their action.<sup>33</sup> The *in silico* ADME computational studies of the target thymol-1,2,3-triazole hybrids were performed using Swiss ADME prediction tools.<sup>34</sup> All the drugs likeness parameters, hydrogen bond acceptor/donor (HBA/HBD), solubility, lipophilicity, topological surface area (TPSA) and percentage of absorption (%ABS) has been determined. The %ABS was obtained by following equation:  $\%ABS = 109 - (0.345 \times TPSA)$ . The obtained results are shown in the Table 1. According to Lipinski's rule of five, any molecules which follow the following parameters i.e. hydrogen bond donors <5, hydrogen bond acceptor <10, molecular weight below 500, calculated log P < 5 can have better *in vivo* absorption

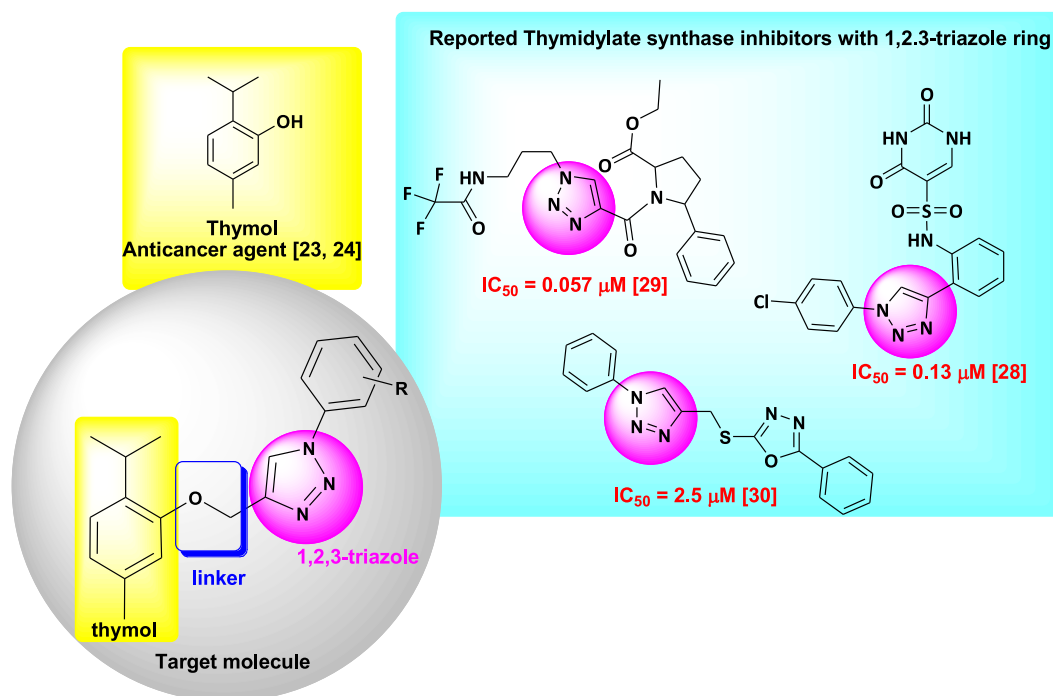
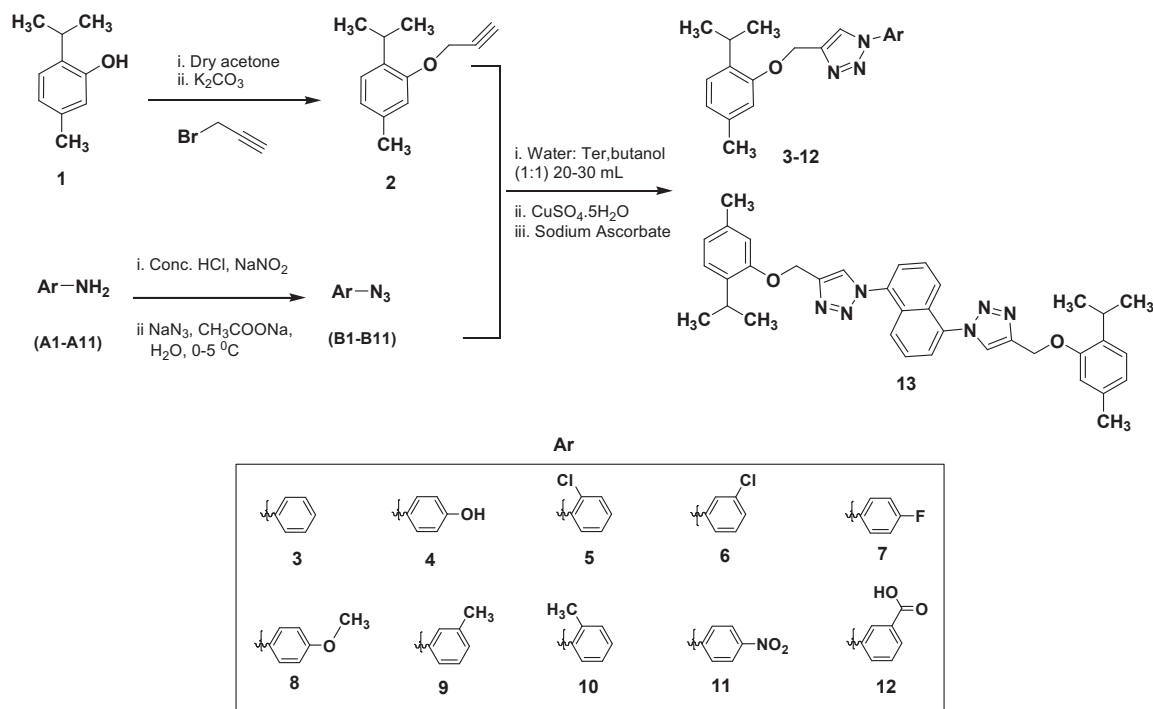


Fig. 1. Drug design for the present work.



Scheme 1. Synthesis of thymol based 1,2,3-triazole hybrids.

Table 1

Pharmacokinetics/ADME predictions of the target compounds 3–13.

Compd. No.	Lipinski parameters					nROTB <sup>e</sup>	TPSA <sup>f</sup>	%ABS <sup>g</sup>	BBB <sup>h</sup>	GI ABS <sup>i</sup>
	MW <sup>a</sup>	HBA <sup>b</sup>	HBD <sup>c</sup>	LogP <sup>d</sup>	Violations					
3	307.39	3	0	3.65	0	5	91.88	77.30	Yes	High
4	323.39	4	1	3.25	0	5	93.91	76.60	Yes	High
5	341.83	3	0	3.82	0	5	96.89	75.57	Yes	High
6	341.83	3	0	3.95	0	5	96.89	75.57	Yes	High
7	325.38	4	0	3.68	0	5	91.84	77.31	Yes	High
8	337.42	4	0	4.05	0	6	98.38	75.05	Yes	High
9	337.42	4	0	3.8	0	6	98.38	75.05	Yes	High
10	321.42	3	0	3.77	0	5	96.85	75.58	Yes	High
11	352.39	5	0	3.2	0	6	100.71	74.25	No	High
12	351.40	5	1	3.27	0	6	98.84	74.90	Yes	High
13	586.73	6	0	5.93	2	10	174.83	48.68	No	Low

<sup>a</sup> Molecular weight.<sup>b</sup> Hydrogen Bond Acceptor.<sup>c</sup> Hydrogen Bond Donor.<sup>d</sup> Partition Coefficient.<sup>e</sup> Number of rotatable bonds.<sup>f</sup> Topological Polar Surface Area.<sup>g</sup> Absorption %.<sup>h</sup> Blood Brain Barrier.<sup>i</sup> Gastro-intestinal absorption.

and bioavailability.<sup>35</sup> Compounds violating more than one of the above rules could have problem in bioavailability.

From the computational ADME results, it was observed that all the final hybrids except compound **13** (-5.93) exhibited Log P less than five (3.20–4.05) indicating good cell permeability. All the hybrids except compound **13** (MW 586) has molecular weight < 500 suggesting easy transportation and absorption. Furthermore, the number of hydrogen bond acceptors and donors present in the final hybrids were <5 and 10, respectively, thus comply with Lipinski rules. The percentage absorption of all the conjugates were above 74% except compound **13** which showed 48.68%, suggests that compound **3–12** should be easily absorbed by human body. From these results, compound **3–12** possess good pharmacokinetics properties and could be used as lead drug candidates.

### 2.3. Biological activities

#### 2.3.1. Cytotoxicity activity

The synthesized thymol linked 1,2,3-triazole **3–13** has been screened for their cytotoxicity in MCF-7 and MDA-MB-231 by MTT assay (Table 2) and the results were compared to 5-fluorouracil (5FU) and Tamoxifen.

Among the tested hybrids, compound **10** (IC<sub>50</sub> 6.17 μM) bearing methyl group at *ortho* position was the most potent compound which showed comparable cytotoxicity to tamoxifen (IC<sub>50</sub> 5.62 μM) and 3.2 times inhibition to 5-FU (IC<sub>50</sub> 20.09 μM) against MCF-7 cancer cells. Compound **5** (IC<sub>50</sub> 15.58 μM) bearing chloro substituents at *ortho* position and compound **12** (IC<sub>50</sub> 10.30 μM) having COOH at *meta* position

**Table 2**

The IC<sub>50</sub> (μM) of the synthesized compounds (3–13) against tested human breast cancer cell line.

Compound No	IC <sub>50</sub> (μM, MCF-7)	IC <sub>50</sub> (μM, MDA-MB-231)
3	29.86 ± 0.27	45.11 ± 1.58
4	45.35 ± 1.82	30.45 ± 0.30
5	<b>15.58 ± 2.40</b>	<b>26.63 ± 1.97</b>
6	32.14 ± 1.11	45.19 ± 1.22
7	22.07 ± 2.38	32.56 ± 1.34
8	25.36 ± 1.21	45.33 ± 1.24
9	28.12 ± 0.45	31.25 ± 0.34
10	<b>6.17 ± 0.46</b>	<b>10.52 ± 1.22</b>
11	32.18 ± 1.74	41.03 ± 1.41
12	<b>10.30 ± 1.83</b>	<b>11.41 ± 0.61</b>
13	<b>18.08 ± 0.16</b>	<b>22.14 ± 1.71</b>
Tamoxifen	5.62 ± 0.20	15.01 ± 0.12
5-fluorouracil (5FU)	20.09 ± 1.12	25.31 ± 0.84

<sup>a</sup>IC<sub>50</sub> values are the concentrations that cause 50% inhibition of cancer cell growth. Data represent the mean values ± standard deviation of three independent experiments performed in triplicate; Breast cancer cells (MCF-7 and MDA-MB-231) were used. Tamoxifen and 5-fluorouracil (5-FU) were used as a reference drugs (positive control).

displayed 1.2- and 1.95- fold activity, respectively to 5FU against the same cancer cells. Compound 13 with naphthyl bridged bis 1,2,3-triazole hybrid revealed promising cell viability with IC<sub>50</sub> 18.08 μM against MCF-7 cancer cells.

It was also found that compound 10 (IC<sub>50</sub> 10.52 μM) and 12 (IC<sub>50</sub> 11.41 μM) were the most active compounds displaying significant inhibition on MDA-MB-231 cells. Compound 10 and 12 revealed 1.42 and 1.3 fold inhibition, respectively to tamoxifen (IC<sub>50</sub> 15.01 μM) whereas they showed 2.4 fold and 2.2 activity to 5FU (IC<sub>50</sub> 25.31 μM). Compounds, 5 and 13 exhibited comparable inhibition to 5FU with IC<sub>50</sub> 26.63 μM and IC<sub>50</sub> 22.14 μM, respectively. Other compounds revealed moderate cytotoxicity with IC<sub>50</sub> in the range 22.07–45.35 μM against MCF-7 and 31.25–45.33 μM against MDA-MB-231 cancer cells. From the cytotoxicity results, compound 10 bearing methyl group at *ortho* position was identified as the most potent compound which displayed significant inhibition against both the tested breast cancer cells (Fig. 2).

The most potent compound 10 was also screened on normal human embryonic kidney cell, HEK 293 cells (non tumorigenic) in order to inquire the selectivity and toxicity on non tumorigenic cells. It was observed from Fig. 3, compound 10 displayed IC<sub>50</sub> > 50 μM against non tumorigenic cells while both the tested breast cancer cells displayed IC<sub>50</sub> 6.1 μM and 10.52 μM, respectively suggesting that compound 10 was found to be selective to MCF-7 and MDA-MB-231 cancer cells and less toxic to non tumorigenic cells.

### 2.3.2. In vitro thymidylate synthase activity

Thymidylate synthase (TS) has evolved as one of the targets for anticancer drugs due to its vital role in chemotherapy. The inhibition of

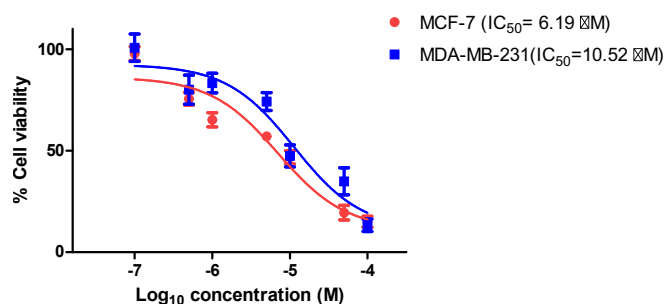


**Fig. 2.** Antiproliferative effect of 10 in MCF-7 and MDA-MB-231 cells. Cell viability was expressed as a percentage of vehicle control [ethanol 0.1% (v/v)] treated cells. The values represent the mean ± S.E.M. for three independent experiments performed in triplicate.

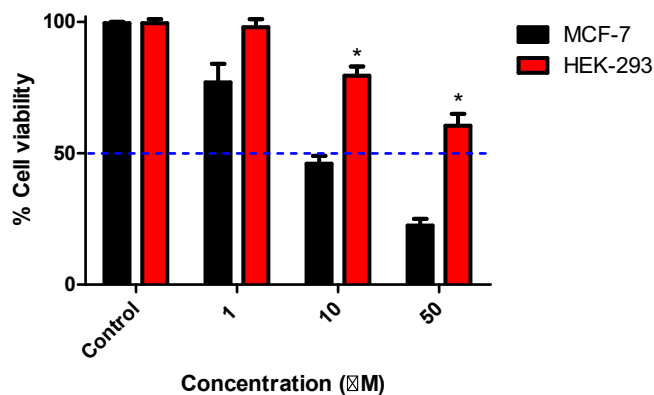


**Fig. 3.** Dose response curve for compound 10 on the proliferation of breast cancer MCF-7 and normal HEK-293 cells. Cells were treated at the indicated concentrations for 72 h. Cell viability was expressed as percentage of vehicle control [ethanol 1% (v/v)] treated cells and was measured by MTT assay (average of three independent experiments). Statistical analysis was performed using one-way ANOVA-Bonferroni post-hoc test (\*,  $p < 0.05$ ).

this enzyme arrests cell cycle and induces apoptosis by blocking deoxythymidine monophosphate (dTMP) formation leading to DNA damage.<sup>31,32</sup> In order to know the mode of action, the most potent molecules, 10 and 12 from the antiproliferative activity were evaluated for *in vitro* TS activity. The results are shown in Table 3. It was found that compound 10 (IC<sub>50</sub> 2.21 μM) and 12 (IC<sub>50</sub> 4.27 μM) significantly inhibited TS enzyme with 2.4 and 1.26 fold activity to standard drug, Pemetrexed (IC<sub>50</sub> 5.39 μM). It is evident from the above results that compound 10 and 12 have the potential to inhibit thymidylate synthase causing DNA synthesis disruption and cessation of cell growth.

### 2.3.3. Cell cycle arrest

To further assess the cellular mechanism of action, the most active compound 10 from MTT assay was selected. The normal cell cycle has four stages: G1, S, G2 and M and therefore development of anticancer drug targets specific stage of the cell cycle to treat this devastating disease.<sup>36</sup> Compound 10 (10 μM) for 48 hrs was tested for cell cycle progression in MCF-7 cells using flow cytometry. The distribution of cells along the sub G1 (<2N), S (>2N), G0-G1 (2 N) and G2/M (4 N) phases of the cycle was exhibited in representative cell cycle grid of the stained DNA in Fig. 4. The results of cell cycle progression showed that 37.3% of MCF-7 cells arrests cell cycle at G2/M phase. Compound 10 displayed 21.4% of cell accumulation in sub-G1 phase whereas in control (untreated cells) only 3.7% were observed. These data clearly suggested that compound 10 significantly arrested cell cycle at the G2/M phase.

### 2.3.4. Annexin V/PI apoptosis

Apoptosis is a natural process that plays a vital role in normal development and homeostasis of an organism. It is promising target of cancer therapy as it removes unwanted cells regardless of the type and cause of cancers.<sup>37</sup> To evaluate the induction of apoptosis by compound 10 in MCF-7 cells, an Annexin-V/Propidium iodide (PI) assay was used. In apoptotic cells, due to impaired cell membrane permeability,

**Table 3**

*In vitro* thymidylate synthase (TS) activity of the active compounds 10, 12 and Pemetrexed.

Compounds	IC <sub>50</sub> (μM)
10	2.21 ± 0.69
12	4.27 ± 1.12
Pemetrexed	5.39 ± 0.94

IC<sub>50</sub> values are the mean ± S.D. of three separate experiments. Pemetrexed: reference drug.

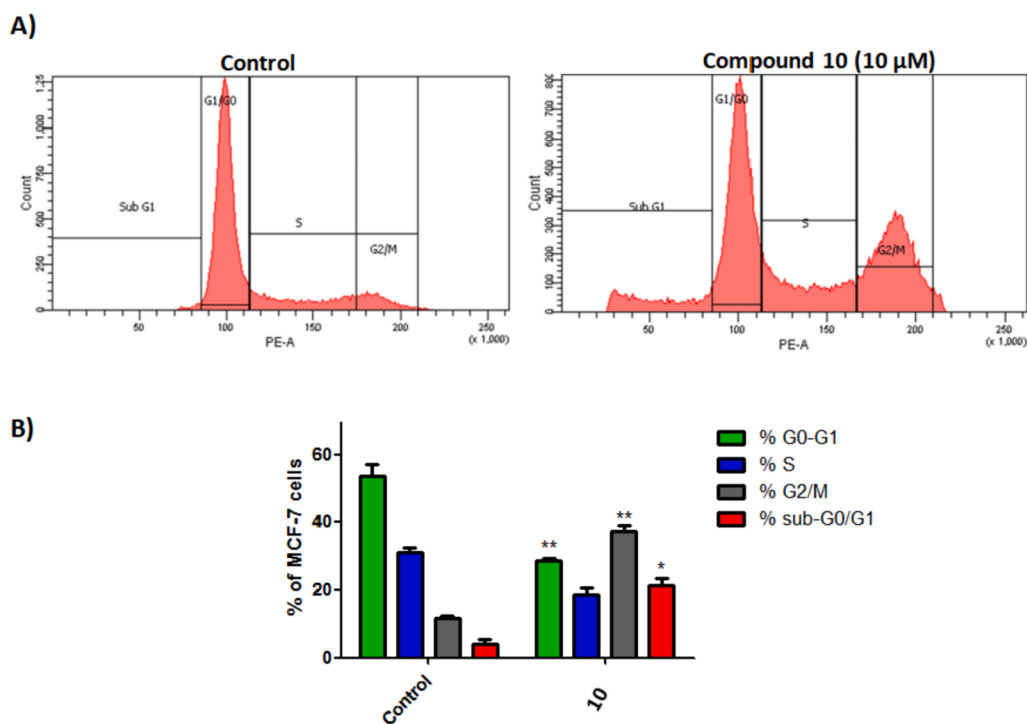


**Fig. 4.** (A) Effect of compound **10** on the cell cycle and apoptosis in breast cancer MCF-7 cells. Cells were treated with either vehicle [0.1% ethanol (v/v)], **10** (10  $\mu$ M) for 48 h. Cells were then fixed, stained with PI, and analyzed by flow cytometry. Cell cycle analysis was performed on histograms of gated counts per DNA area (FL2-A). (B) Quantitative analysis of 4 N (G2/M), 2 N (G0G1), >2N (S) and < 2 N (sub-G1). DNA content was determined with Cell-Quest software. Values represent the mean  $\pm$  SEM for three independent experiments. Statistical analysis was performed using one-way ANOVA-Bonferroni post-hoc test (\*,  $p < 0.05$ ; \*\*,  $p < 0.01$ ).

phosphatidyl serine which acts as a marker of apoptosis is exposed on cell surface and gets detected by Annexin reagent. Whereas the DNA of late apoptotic and necrotic cells gets stain with propidium iodide therefore Annexin-V/Propidium iodide dual staining cause the differentiation between apoptotic (both early and late), live and necrotic cells.

After 48 hrs of treatment of MCF-7 cells with compound **10** at 10  $\mu$ M, the percentage of both early and late apoptotic cells (total) displayed significant increase from 8.3% to 29.4% compared to control cells (Fig. 5). The findings of cell cycle arrest and apoptosis studies indicate that the compound **10** has the potential to kill breast cancer cells through the

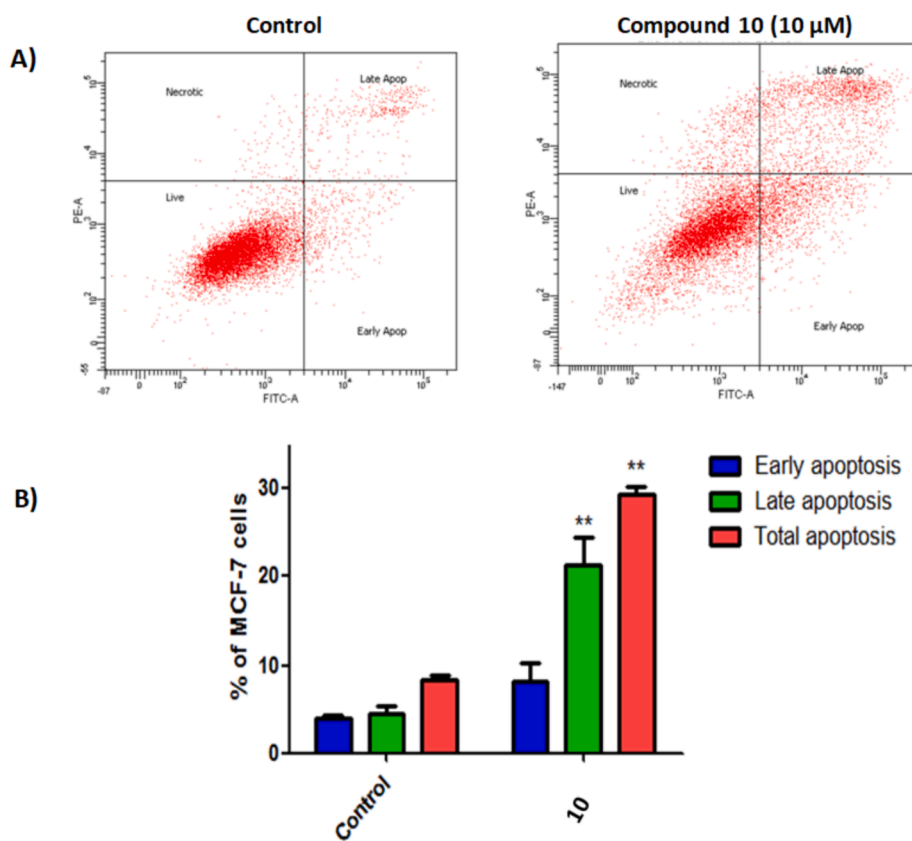


**Fig. 5.** Compound **10** induces apoptosis in breast cancer MCF-7 cells (Annexin V/PI FACS). (A) Effect of compound **10** in MCF-7 cells analysed by flow cytometry after double staining of the cells with Annexin-V-FITC and PI. MCF-7 cells treated with 10  $\mu$ M of compound **10** for 48 h and collected and processed for analysis. (B) Quantitative analysis of apoptosis. Values represent the mean  $\pm$  SEM for three independent experiments. Statistical analysis was performed using one-way ANOVA-Bonferroni post-hoc test (\*\*,  $p < 0.01$ ). The four quadrants identified as: LL, viable; LR, early apoptotic; UR, late apoptotic; UL, necrotic.

inhibition of thymidylate synthase.

## 2.4. Computational studies

### 2.4.1. Molecular docking studies

The docking study was performed to know the possible molecular interactions of the hybrids **3–13** with thymidylate synthase (TS) protein. The crystal structure of TS protein bounded with 5-fluoro-2'-deoxyuridine-5'-monophosphate (FdUMP) was obtained as PDB file (ID 6QXG) with 2.0 Å resolution.<sup>38</sup> The CASTp package identified the active site of TS protein as Asn 226, Asp 218, Arg50, Arg 215, Ser 216 and His 256 residue. The synthesized hybrids **3–13** and 5 fluorouracil (5FU) were redocked into active site in absence of original inhibitor FdUMP. The obtained docked poses were filtered based on the lowest binding free energy  $\Delta G$  and lowest root mean square deviation (RMSD) between the pose before and after refinement (Table 4). All the synthesized compounds showed higher binding affinity (-6.37 to -8.37 Kcal/mol.) than 5 FU (-3.92 Kcal/ mole) and FdUMP (-5.28 Kcal/mol.). The calculated RMSDs were found to be lower than 2° reflecting the accuracy of docking process. The potent compounds **10** and **12** from biological activity displayed nearly same binding affinity ( $-7.07 \pm 0.25$  and  $-6.96 \pm 0.16$  Kcal/mol.), respectively. The lowest RMSD of 0.98 for compound **10** among all the synthesized compounds may be explaining raising efficiency for this compound (Table 4).

It was found that compound **10** stabilized in TS binding pocket through arrangement of thymol cluster in perpendicular mode to form  $\pi$ - $\pi$  cation interaction with Arg 215 and H-bonding with Tyr 258 residue of the protein (Fig. 6). Whereas compound **12**, bearing carboxyl group at meta position, make it more flexible thereby exhibiting significantly higher score and interaction with Arg 215, Arg 175 and Arg 176 residue of the protein (Fig. 7). These data represents a circular interaction for compounds **3–13**, 5FU and FdUMP into the TS pocket that promises a suitable filling for this part of enzyme. These results support our biological activities results.

### 2.4.2. Orientation structure based on computational study

The critical features connected to biological properties for tested compounds were calculated at DFT theory,<sup>39,40</sup> using exchangeable B<sub>3</sub>LYP/6311G\*\* correlation function<sup>41</sup> through MIDX basis set.<sup>42</sup> The optimization structures for ligands (**3–13**) have been obtained from DFT simulations and represented in Fig. 8. It was found that thymol cluster showed planarity arrangement with triazole linker in **3–5** and **11**. While in other members **6–10**, **12** and **13** their rings were arranged in the perpendicular mode.

All calculated DFT features are related to analysis of frontier molecular orbitals FMOs. That is abiotic orbital for determination of stability and reactivity of biomolecules in biological system. HOMO and

LUMO are impacted in FMO, these concepts referred to High occupied and low unoccupied molecular orbitals, respectively. The energy for HOMO, LUMO and gap between FMOs orbitals were calculated ( $E_{\text{HOMO}}$ ,  $E_{\text{LUMO}}$  and  $\Delta G$ ). These parameters are important to discover vital characters as, I: Ionization-potential, A; electron-affinity;  $\eta$ : Hardness (eV),  $\delta$ : Softness(eV),  $\chi$ : Electronegativity (eV),  $\omega$ : electrophilicityindex;  $\mu^+$ : ability for electron accepting,  $\mu^-$ : electron donating power,  $\omega^\pm$ : group philicity(eV);  $\Delta N_{\text{max}}$ : transfer of a maximum amount of electrons, (Table 5). The calculated parameters were represented equationally. (Eqs. S1–S11, supplementary materials). The most potent compounds **10** and **12** showed lowest  $\Delta G$  values among all the target compounds. It can be observed from Table 5, these two compounds displayed the highest values for most of the chemical descriptors ( $\delta$ ,  $\chi$ ,  $\omega$ ;  $\mu^+$ ,  $\mu^-$ ,  $\omega^\pm$ ;  $\Delta N_{\text{max}}$ ) as well as lower rigidity (5.72 & 5.65 ev.) respectively, thereby reflecting higher reactivity for **10** and **12**. The group philicity " $\omega^\pm$ " was used to study intermolecular charge transfer between biomolecule and biological media. The positive values of  $\omega^\pm$  for compounds **11** & **12** revealed that these two compounds occupy the binding site through a nucleophilic attack.

From Fig. 9, it can be observed that HOMO zones have been occupied by thymol ring for all compounds **3–13**. Whereas the LUMO areas have been condensed in phenyl 1-(derivatives)-1H-1,2,3-triazole scaffolds in all compounds (Fig. 10). This data helped us to elucidate the intramolecular charge transfer between HOMO  $\rightarrow$  LUMO of thymol to triazole scaffolds.

### 2.4.3. Molecular electrostatic potential (MEP) analysis

The MEP (molecular electrostatic potential) map initially performed to investigate the electrons distribution on the reactive molecular sites, and then predict the interaction manner of the molecule as well as physicochemical descriptors relationships.<sup>43</sup> Furthermore, MEP introduces a balance between both repulsive interaction of the nuclei (positive charge as nucleophilic reactivity in blue color) and attractive interaction of the electrons (negative charge as electrophilic potency in yellow and red colors). Green color was visualized as an intermediate potential value. The distribution of colors on MEPs exhibits the difference at electrostatic potential values, which their increases in the order red < yellow < blue < green (Fig. 11). It is supported that the orientation of the molecules based on size and shape. The maximum green regions are shielded upon phenyl rings in all compounds, while the yellow zones are localized at triazole sites. The variation of colors providing one a helpful identification about how the molecular sites able to form intermolecular interactions, as well as where is most sensitive sites undergoing electrophilic and nucleophilic attack. Furthermore, raising blue region may be explained by a high electrophilic ability for its compounds, which are responsible for the substrate ability to recognize the binding site through electrostatic force between substrate

**Table 4**

Binding energies of the synthesized compounds against human Thymidylate synthase protein 6QXG.

Compd	$\Delta G$	RMSD	Int.	H.B.	E. ele	Evdw	LE
3	-6.96 $\pm$ 0.61	1.80	-34.41	-13.49	-11.28	-38.32	-3.87
4	-6.86 $\pm$ 0.29	1.02	-28.65	-18.33	-9.33	-35.48	-3.39
5	-6.54 $\pm$ 0.13	1.01	-29.65	-15.10	-9.48	-33.25	-3.25
6	-7.20 $\pm$ 0.64	1.50	-26.94	-18.26	-9.19	-31.34	-2.88
7	-8.37 $\pm$ 0.61	1.63	-65.05	-10.46	-7.92	-42.56	-3.18
8	-6.74 $\pm$ 0.58	1.49	-29.56	-6.51	-13.49	-44.17	-2.71
9	-6.80 $\pm$ 0.41	1.50	-70.12	-14.03	-9.47	-35.45	-2.72
10	-7.07 $\pm$ 0.25	0.98	-36.34	-16.27	-9.02	-32.04	-3.14
11	-6.92 $\pm$ 0.37	1.35	-49.54	-16.48	-9.59	-25.03	-2.97
12	-6.96 $\pm$ 0.16	1.06	-87.11	-7.86	-13.74	-40.76	-4.26
13	-6.37 $\pm$ 0.32	2.63	-65.05	-10.46	-7.92	-42.56	-3.10
5FU	-3.92 $\pm$ 0.07	1.71	-75.34	-66.58	-7.60	-6.76	-2.29
FdUMP	-5.28 $\pm$ 0.15	1.60	-433.91	-21.32	-17.47	-58.37	-3.30

$\Delta G$ : Free binding energy of the ligand from a given conformer, Int.: Affinity binding energy of hydrogen bond interaction with receptor, H.B.: Hydrogen bonding energy between protein and ligand, Eele: Electrostatic interaction with the receptor, Evdw: Van der Waals energies between the ligand and the receptor, L.E.: Ligand efficiency. Excel was used to apply Mean  $\pm$  SD test for the analyses of the ligand efficiency \* = statistically significant at 5% level.

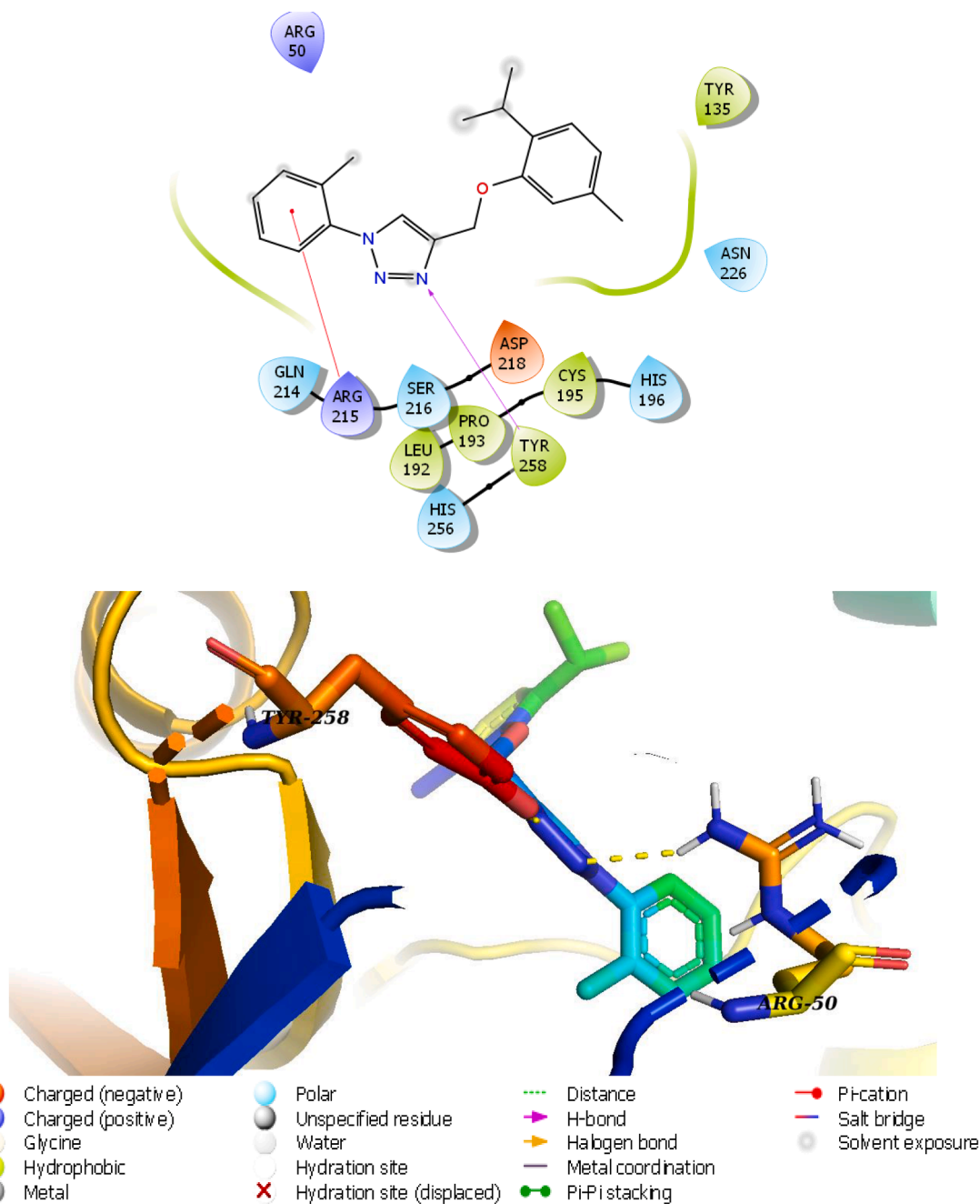


Fig. 6. Molecular docking of the active compounds **10** against Thymidylate synthase protein (6QXG).

and receptor.

### 3. Conclusions

In the present work, thymol linked 1,2,3-triazole hybrids have been synthesized and evaluated for anticancer activities. The synthesized molecules displayed desired pharmacokinetic properties for an orally available drug. Two compounds, compound **10** ( $IC_{50}$  10.52  $\mu$ M) and **12** ( $IC_{50}$  11.41  $\mu$ M) were the most active compounds displaying 1.42 and 1.3 fold inhibition, respectively to tamoxifen ( $IC_{50}$  15.01  $\mu$ M) whereas 2.4 fold and 2.2 activity to 5FU ( $IC_{50}$  25.31  $\mu$ M) on MDA-MB-231. Against MCF-7 cancer cells, compound **10** ( $IC_{50}$  6.17  $\mu$ M) was the most potent compound which showed comparable cytotoxicity to tamoxifen ( $IC_{50}$  5.62  $\mu$ M) and 3.2 times activity to 5-FU ( $IC_{50}$  20.09  $\mu$ M). Furthermore, **10** and **12** significantly inhibited thymidylate synthase

enzyme with 2.4 and 1.26 fold activity to standard drug, Pemetrexed ( $IC_{50}$  5.39  $\mu$ M) indicating their mode of action as TS inhibitors. Cell cycle arrest and annexin V induced apoptosis study of compound **10** in MCF-7 cells showed cell cycle arrest at the G2/M and induction of apoptosis. The molecular docking simulations showed that the synthesized compounds have high ability interaction with TS protein. The DFT study was used for emphasized the molecular docking and experimental findings. FMOs studies demonstrated the effect of HOMO orbitals on charge transfer from thymol to TS receptors. The calculated chemical reactivity and MEP demonstrated that high electrophilic behavior for compound **10** and **12** were impact on recognition power between the substrate and TS binding site. Therefore, compound **10** could be served as a lead molecule for the treatment of breast cancer.

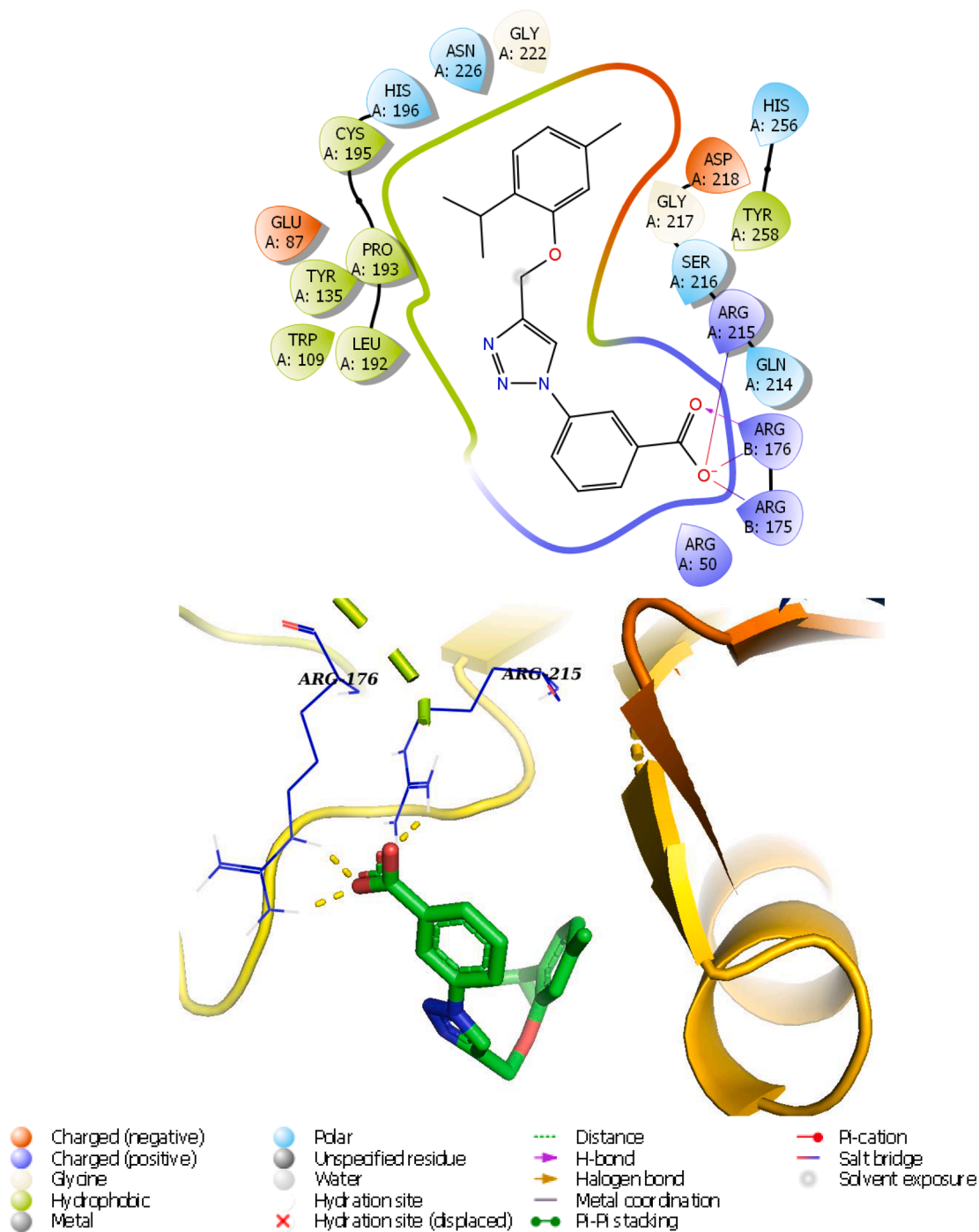


Fig. 7. Molecular docking of the active compounds 12 against Thymidylate synthase protein (6QXG).

## 4. Experimental

### 4.1. Chemistry

The chemicals and reagents required for this work were purchased from Sigma Aldrich (Germany), Across (USA) and Loba Chem (India) and were used as such. The synthesized compounds were confirmed by different analytical techniques. Melting point of the compounds was measured on the electrothermal melting point apparatus (Stuart SMP40). FT IR analysis was performed on Thermo Scientific iS 50 by Attenuated Total Reflectance method. Nuclear Magnetic Resonance analysis was performed on Bruker (850 MHz) in  $CDCl_3$  using tetramethylsilane (TMS) as internal reference. The Chemical shift ( $\delta$ ) reported in

part per million (ppm) and coupling constant ( $J$ ) in Hertz (Hz). LECO Elemental Analyzer was used for elemental analysis. Thermo Scientific LCQ Fleet (LCF10605) mass spectrometer was used for determination of their molecular mass using electron spray ionization (ESI) method and provided in  $m/z$ .

#### 4.1.1. Synthesis of 1-isopropyl-4-methyl-2-(prop-2-ynyloxy)benzene (2)

In a dry and clean round bottom flask (250 mL) was charged thymol (0.02 mol), dry acetone (100 mL) and anhydrous potassium carbonate (0.03 mol). The combined mixture was refluxed for 1 hr and then allowed to cool at 20–30 °C. Then propargyl bromide (0.02 mol) was charged into the reaction mixture and further stirred at 50–60 °C for 5 hrs. After completion of the reaction monitored by TLC, was filtered in

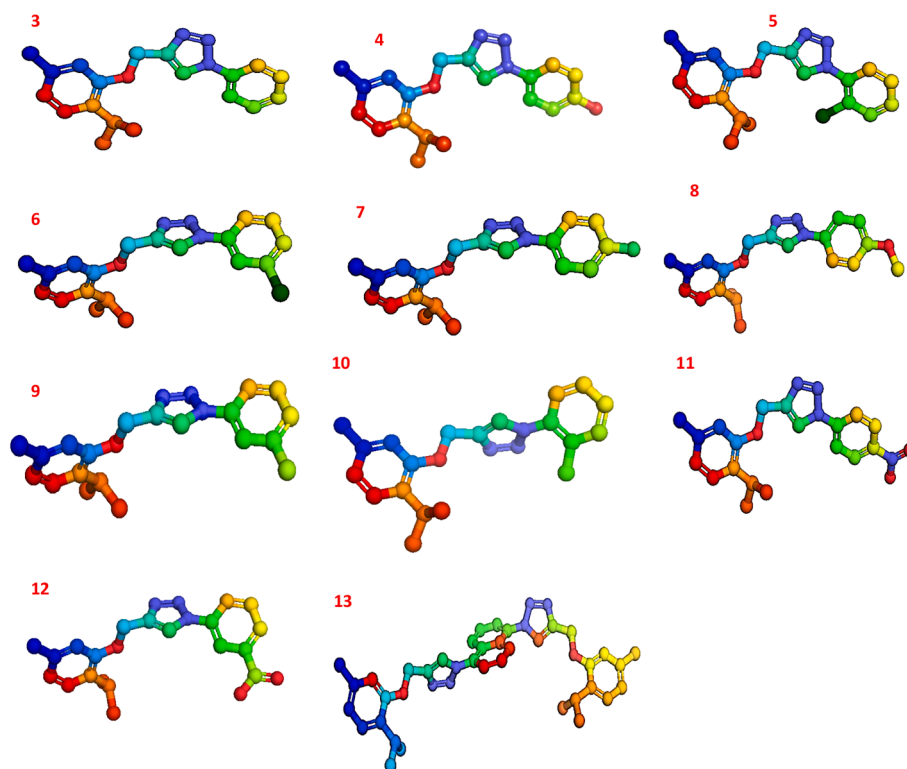


Fig. 8. Optimized geometrical structures of synthesized compounds (3–13).

Table 5

Calculated chemical reactivity parameters for compounds (3–13) at DFT with a B3LYP/6-311G\*\* Basics sets.

	3	4	5	6	7	8	9	10	11	12	13
$E_{HOMO}$	-8.37	-8.42	-8.29	-8.37	-8.43	-8.34	-8.35	-8.41	-8.47	-8.34	-8.66
$E_{LUMO}$	2.67	2.26	2.48	1.6	2.51	2.92	2.7	3.03	0.69	2.96	1.9
$\Delta G$	-11.04	-10.68	-10.77	-9.97	-10.94	-11.26	-11.05	-11.44	-9.16	-11.30	-10.56
$\eta$	5.52	5.34	5.39	4.99	5.47	5.63	5.53	5.72	4.58	5.65	5.28
$\delta$	0.18	0.19	0.19	0.20	0.18	0.18	0.18	0.17	0.22	0.18	0.19
$\chi$	-2.85	-3.08	-2.91	-3.39	-2.96	-2.71	-2.83	-2.69	-3.89	-2.69	-3.38
EP	2.85	3.08	2.91	3.39	2.96	2.71	2.83	2.69	3.89	2.69	3.38
$\omega_i$	0.74	0.89	0.78	1.15	0.80	0.65	0.72	0.63	1.65	0.64	1.08
I	8.37	8.42	8.29	8.37	8.43	8.34	8.35	8.41	8.47	8.34	8.66
A	-2.67	-2.26	-2.48	-1.60	-2.51	-2.92	-2.70	-3.03	-0.69	-2.96	-1.90
$\mu^+$	2.90	3.32	3.02	3.99	3.08	2.66	2.86	2.61	5.25	2.63	3.85
$\mu^-$	-5.61	-5.75	-5.60	-5.88	-5.70	-5.53	-5.59	-5.55	-6.18	-5.52	-6.02
$\omega^\pm$	-0.09	-0.41	-0.21	-0.89	-0.23	0.11	-0.06	0.17	-1.60	0.14	-0.74
$\Delta N_{max}$	0.52	0.58	0.54	0.68	0.54	0.48	0.51	0.47	0.85	0.48	0.64

hot condition, washed with hot acetone (30 mL). To the filtrate after concentration was added water and dichloromethane (50 mL), organic layer was separated and dried over anhydrous sodium sulphate. Dichloromethane was completely evaporated under reduced pressure to get light yellow liquid of O-propargylated thymol (2)

IR (ATR)  $\nu$   $\text{cm}^{-1}$ : 3291, 2960, 2121, 1612, 1504, 1244, 1209, 1035, 810

ESI Mass: 189 [M+H]<sup>+</sup>

#### 4.1.2. General procedure for synthesis of 4-((2-isopropyl-5-methylphenoxy)methyl)-1-(substitutedaryl)-1H-1,2,3-triazole (3–13)

O-propargylated thymol 2 (0.0013 mol) and tertiary butanol:water (1:1, 20–40 mL) was charged to 100 mL RBF, heated slightly to get clear solution. Aqueous copper sulphate pentahydrate (0.0013 mol, 5 mL) and aqueous sodium ascorbate (0.0013 mol, 5 mL) was added to it and stirred at 20–30 °C for 30–40 mins. Then aromatic azides (0.0015 mol) was added and the reaction mixture was continued on stirring at 20–30 °C for 3–14 hrs. The reaction was monitored by TLC, after disappearance

of the starting material, water (50 mL) was charged and the product was extracted with dichloromethane (50–60 mL). The combined organic layer was washed with brine solution (50 mL) and dried over anhydrous sodium sulphate. Dichloromethane was evaporated and the products were recrystallized in dichloromethane and cyclohexane to yield compounds 3–13 (yield 60–90%).

4.1.2.1. 4-((2-isopropyl-5-methylphenoxy)methyl)-1-phenyl-1H-1,2,3-triazole (3). Yield 74%; creamy crystals; M.p.: 77–78 °C; IR (ATR)  $\nu$   $\text{cm}^{-1}$ : 3110, 2954, 1599, 1502, 1410, 1288, 1252, 1212, 1166, 1063, 1035; <sup>1</sup>H NMR (850 MHz, CDCl<sub>3</sub>)  $\delta$  ppm: 1.24–1.25 (m, 6H, Ar-CH(CH<sub>3</sub>)<sub>2</sub>), 2.37 (s, 3H, Ar-CH<sub>3</sub>), 3.34–3.37 (m, 1H, Ar-CH(CH<sub>3</sub>)<sub>2</sub>), 5.32 (s, 2H, O-CH<sub>2</sub>-), 6.83 (d,  $J$  = 8.5 Hz, 1H, Ar-H), 6.89 (br.s, 1H, Ar-H) 7.16 (d,  $J$  = 8.5 Hz, 1H, Ar-H) 7.49 (br.s, 1H, Ar-H), 7.57 (t,  $J$  = 8.50 Hz, 2H, Ar-H), 7.81 (d,  $J$  = 8.50 Hz, 2H, Ar-H), 8.33 (br.s, 1H, triazole proton); <sup>13</sup>C NMR (214 MHz, CDCl<sub>3</sub>)  $\delta$  ppm: 21.45, 22.86, 26.62, 62.26, 112.82, 120.86, 122.00, 126.10, 128.89, 129.94, 134.30, 136.60, 155.26. ESI MS: 308 [M+H]<sup>+</sup> C<sub>19</sub>H<sub>21</sub>N<sub>3</sub>O (Calcd): C, 74.24; H, 6.89; N,

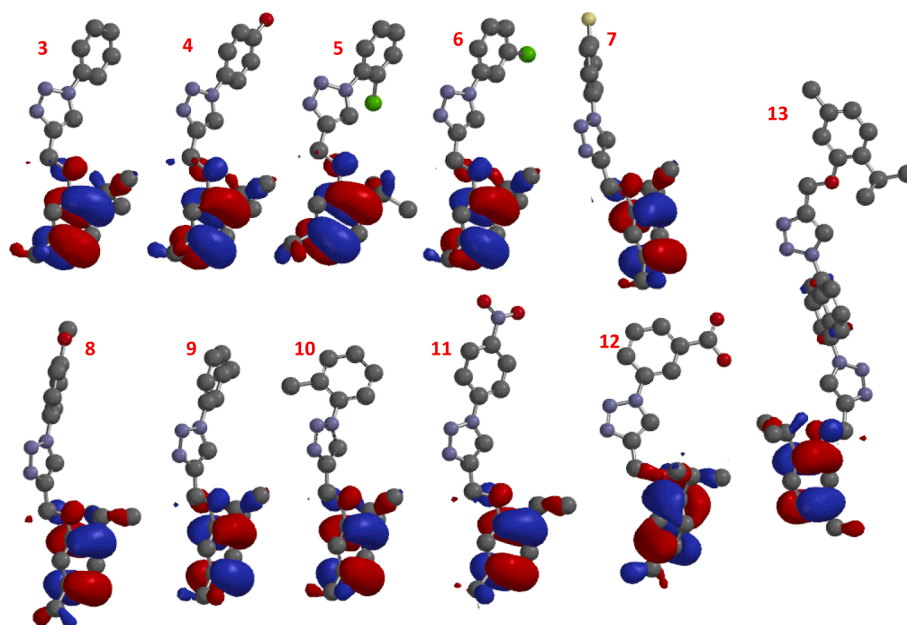


Fig. 9. Plotting the molecular orbital for HOMO for 3–13 molecules based on DFT.

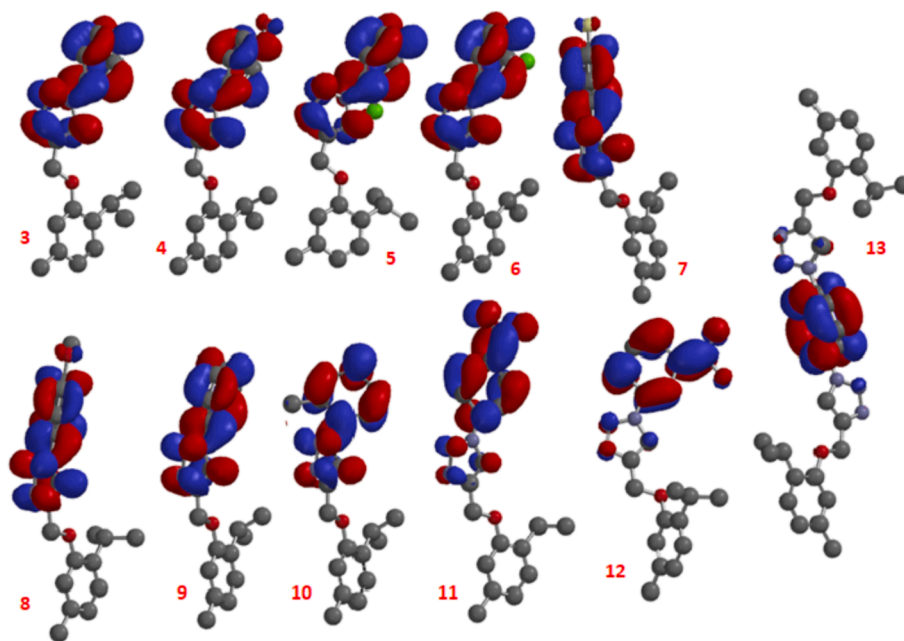


Fig. 10. Plotting the molecular orbital for LUMO for 3–13 molecules based on DFT.

13.67; O, 5.20. Obsd:C, 74.22; H, 6.90; N, 13.65; O, 5.21

4.1.2.2. 4-(4-((2-isopropyl-5-methylphenoxy)methyl)-1H-1,2,3-triazol-1-yl)phenol (**4**). Yield 68%; Creamy granules; M.p.: 88–89 °C; IR (ATR)  $\nu_{\text{cm}^{-1}}$ : 3215, 3061, 2957, 1599, 1518, 1461, 1409, 1384, 1282, 1254, 1226, 1186, 1055;  $^1\text{H}$  NMR (850 MHz,  $\text{CDCl}_3$ )  $\delta$  ppm: 1.02 (d,  $J = 7.27$ , 6H, Ar-CH( $\text{CH}_3$ )<sub>2</sub>), 2.29 (s, 3H, Ar-CH<sub>3</sub>), 3.17–3.20 (m, 1H, Ar-CH( $\text{CH}_3$ )<sub>2</sub>), 5.19 (s, 2H, O-CH<sub>2</sub>-), 6.74 (d,  $J = 7.27$  Hz, 1H, Ar-H), 7.94–7.96 (m, 2H, Ar-H), 7.0 (s, Hz, 1H, Ar-H), 7.06 (d,  $J = 7.78$  Hz, 1H, Ar-H), 7.62–7.70 (m, 2H, Ar-H), 8.74 (s, 1H, Triazole proton), 9.99 (s, 1H, Ar-OH);  $^{13}\text{C}$  NMR (214,  $\text{CDCl}_3$ )  $\delta$  ppm: 21.42, 22.85, 26.59, 62.18, 100.0, 112.80, 116.45, 121.99, 122.72, 126.10, 134.28, 136.60, 155.26, 157.23. ESI MS: 324  $[\text{M}+\text{H}]^+$   $\text{C}_{19}\text{H}_{21}\text{N}_3\text{O}_2$ (Calcd): C, 70.57; H, 6.55; N, 12.99; O, 9.89. Obsd:C, 70.54; H, 6.56; N, 12.97; O, 9.90.

4.1.2.3. 4-((2-isopropyl-5-methylphenoxy)methyl)-1-(2-chlorophenyl)-1H-1,2,3-triazole (**5**). Yield 65%; white powder; M.p.: 62–63 °C; IR (ATR)  $\nu_{\text{cm}^{-1}}$ : 3084, 2954, 1609, 1578, 1496, 1448, 1383, 1288, 1246, 1029, 806;  $^1\text{H}$  NMR (850 MHz,  $\text{CDCl}_3$ )  $\delta$  ppm: 1.23–1.26 (m, 6H, Ar-CH( $\text{CH}_3$ )<sub>2</sub>); 2.38 (s, 3H, Ar-CH<sub>3</sub>), 3.33–3.36 (m, 1H, Ar-CH( $\text{CH}_3$ )<sub>2</sub>), 5.35 (br.s, 2H, O-CH<sub>2</sub>-), 6.83 (d,  $J = 8.5$  Hz, 1H, Ar-H), 6.89 (br.s., 1H, Ar-H), 7.15 (d,  $J = 8.5$  Hz, 1H, Ar-H), 7.49–7.50 (m, 2H, Ar-H), 7.63–7.66 (m, 1H, Ar-H), 7.69 (br.s, 1H, Ar-H), 8.28 (br.s, 1H, triazole proton);  $^{13}\text{C}$  NMR (214 MHz,  $\text{CDCl}_3$ )  $\delta$  ppm: 21.43, 22.83, 26.70, 62.34, 112.93, 122.00, 126.12, 127.82, 128.01, 128.72, 130.86, 134.35, 136.56, 155.28. ESI MS: 342  $[\text{M}+\text{H}]^+$ , 344  $[\text{M}+2+\text{H}]^+$   $\text{C}_{19}\text{H}_{20}\text{ClN}_3\text{O}$  (Calcd): C, 66.76; H, 5.90; N, 12.29; O, 4.68. Obsd:C, 66.74; H, 5.91; N, 12.28; O, 4.69.

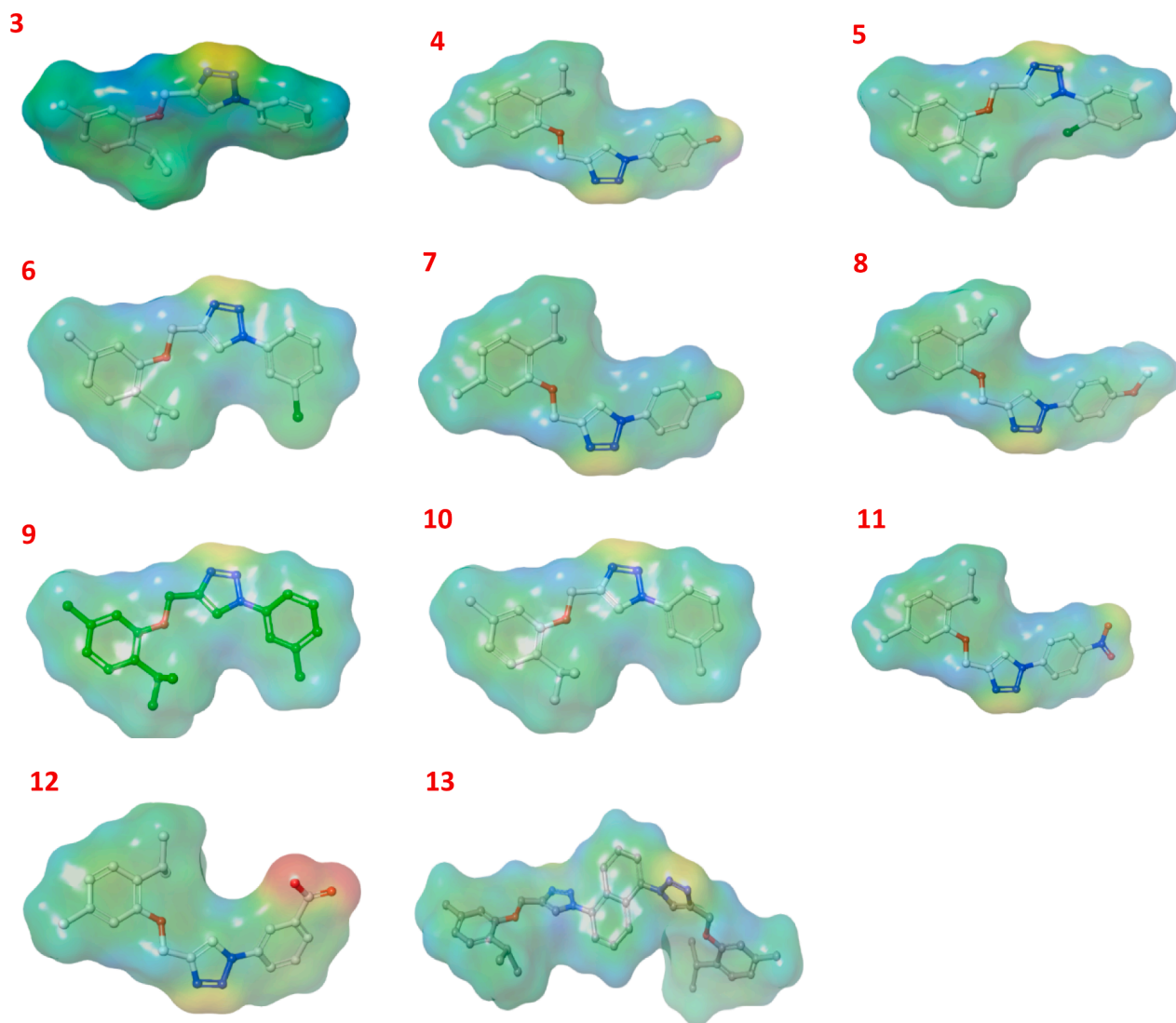


Fig. 11. MEP for the synthesized compounds (3–13) at DFT/6311G\*\*.

4.1.2.4. 4-((2-isopropyl-5-methylphenoxy)methyl)-1-(3-chlorophenyl)-1H-1,2,3-triazole (6). Yield 74%; white powder, M.p.: 71–72 °C. IR (ATR)  $\nu_{\text{cm}^{-1}}$ : 3080, 2961, 1595, 1488, 1256, 1238, 1156, 1091, 808, 784;  $^1\text{H}$  NMR (850 MHz,  $\text{CDCl}_3$ )  $\delta$  ppm: 1.25 (br.s, 6H, Ar-CH( $\text{CH}_3$ )<sub>2</sub>), 2.37 (s, 3H, Ar-CH<sub>3</sub>), 3.35–3.36 (m, 1H, Ar-CH( $\text{CH}_3$ )<sub>2</sub>), 5.32 (br.s, 2H, O-CH<sub>2</sub>-), 6.84 (d,  $J$  = 8.50 Hz, 1H, Ar-H), 6.87 (br.s, 1H, Ar-H), 7.17 (d,  $J$  = 8.50 Hz, 1H, Ar-H), 7.46 (d,  $J$  = 8.50 Hz, 1H, Ar-H), 7.50 (t,  $J$  = 7.79 Hz, 1H, Ar-H), 7.70 (d,  $J$  = 8.5 Hz, 1H, Ar-H), 7.85 (br.s, 1H, Ar-H), 8.23 (br.s, 1H, triazole proton);  $^{13}\text{C}$  NMR (214 MHz,  $\text{CDCl}_3$ )  $\delta$  ppm: 21.43, 22.73, 26.86, 62.47, 112.92, 122.12, 126.11, 127.62, 128.03, 128.35, 130.29, 134.27, 136.72, 155.34. ESI MS: ESI MS: 342 [M+H]<sup>+</sup>, 344 [M+2+H]<sup>+</sup> C<sub>19</sub>H<sub>20</sub>ClN<sub>3</sub>O (Calcd): C, 66.76; H, 5.90; N, 12.29; O, 4.68. Obsd: C, 66.75; H, 5.91; N, 12.28; O, 4.69

4.1.2.5. 4-((2-isopropyl-5-methylphenoxy)methyl)-1-(4-fluorophenyl)-1H-1,2,3-triazole (7). Yield 82%; Creamy flakes; M.p.: 104–106 °C; IR (ATR)  $\nu_{\text{cm}^{-1}}$ : 3069, 2964, 1513, 1456, 1407, 1253, 1229, 1165, 1022, 837, 810;  $^1\text{H}$  NMR (850 MHz,  $\text{CDCl}_3$ )  $\delta$  ppm: 1.24 (d,  $J$  = 6.75 Hz, 6H, Ar-CH( $\text{CH}_3$ )<sub>2</sub>), 2.37 (s, 3H, Ar-CH<sub>3</sub>), 3.33–3.35 (m, 1H, Ar-CH( $\text{CH}_3$ )<sub>2</sub>), 5.32 (br.s, 2H, O-CH<sub>2</sub>-), 6.83 (d,  $J$  = 8.50 Hz, 1H, Ar-H), 6.87 (s, 1H, Ar-H), 7.16 (d,  $J$  = 8.50 Hz, 1H, Ar-H), 7.26 (t,  $J$  = 8.56 Hz, 2H, Ar-H), 7.76 (dd,  $J$  = 9.08, 4.41 Hz, 2H, Ar-H), 8.11 (br.s, 1H, triazole proton);  $^{13}\text{C}$  NMR (214 MHz,  $\text{CDCl}_3$ )  $\delta$  ppm: 21.42, 22.86, 26.61,

62.31, 112.77, 116.78, 122.02, 122.72, 126.13, 134.28, 136.61, 155.23, 163.08; ESI MS: 326[M+H]<sup>+</sup> C<sub>19</sub>H<sub>20</sub>FN<sub>3</sub>O (Calcd): C, 70.13; H, 6.20; N, 12.91; O, 4.92. Obsd: C, 70.10; H, 6.21; N, 12.90; O, 4.93.

4.1.2.6. 4-((2-isopropyl-5-methylphenoxy)methyl)-1-(4-methoxyphenyl)-1H-1,2,3-triazole (8). Yield 83%; White powder; M.p.: 86–87 °C; IR (ATR)  $\nu_{\text{cm}^{-1}}$ : 3074, 2957, 1516, 1504, 1452, 1410, 1251, 1164, 1019, 831, 807;  $^1\text{H}$  NMR (850 MHz,  $\text{CDCl}_3$ )  $\delta$  ppm: 1.23 (br.s, 6H, Ar-CH( $\text{CH}_3$ )<sub>2</sub>), 2.36 (s, 3H, Ar-CH<sub>3</sub>), 3.33–3.36 (m, 1H, Ar-CH( $\text{CH}_3$ )<sub>2</sub>), 3.90 (s, 3H, OCH<sub>3</sub>), 5.31 (br.s, 2H, O-CH<sub>2</sub>-), 6.82 (d,  $J$  = 8.50 Hz, 1H, Ar-H), 6.87 (s, 1H, Ar-H), 7.06 (d,  $J$  = 8.50 Hz, 1H, Ar-H), 7.15 (d,  $J$  = 8.50 Hz, 1H, Ar-H), 7.69 (br.s., 2H, Ar-H), 8.09 (br.s, 1H, triazole proton);  $^{13}\text{C}$  NMR (214 MHz,  $\text{CDCl}_3$ )  $\delta$  ppm: 21.42, 22.86, 26.59, 55.69, 62.32, 112.80, 114.86, 116.66, 121.98, 122.44, 126.10, 134.29, 136.59, 155.27, 159.95; ESI MS: 338[M+H]<sup>+</sup> C<sub>20</sub>H<sub>23</sub>N<sub>3</sub>O<sub>2</sub> (Calcd): C, 71.19; H, 6.87; N, 12.45; O, 9.48. Obsd: C, 71.17; H, 6.88; N, 12.45; O, 9.49.

4.1.2.7. 4-((2-isopropyl-5-methylphenoxy)methyl)-1-*m*-tolyl-1H-1,2,3-triazole (9). Yield 74%; white powder, M.p.: 65–66 °C; IR (ATR)  $\nu_{\text{cm}^{-1}}$ : 2905, 1610, 1503, 1455, 1408, 1290, 1251, 1170, 1092, 1043, 1030, 788;  $^1\text{H}$  NMR (850 MHz,  $\text{CDCl}_3$ )  $\delta$  ppm: 1.24 (d,  $J$  = 8.50 Hz, 6H, Ar-CH( $\text{CH}_3$ )<sub>2</sub>), 2.37 (s, 3H, Ar-CH<sub>3</sub>), 2.49 (s, 3H, Ar-CH<sub>3</sub>), 3.34–3.37 (m, 1H, Ar-CH( $\text{CH}_3$ )<sub>2</sub>), 5.31 (br.s., 2H, O-CH<sub>2</sub>-), 6.83 (d,  $J$  = 8.50

Hz, 1H, Ar—H), 6.89 (br.s., 1H, Ar—H), 7.16 (d,  $J = 8.50$  Hz, 1H, Ar—H), 7.29–7.30 (m, 1H, Ar—H), 7.44 (t,  $J = 8.50$  Hz, 1H, Ar—H), 7.57 (d,  $J = 8.50$  Hz, 1H, Ar—H), 7.65 (br.s., 1H, Ar—H), 8.39 (br.s., 1H, triazole proton).  $^{13}\text{C}$  NMR (214 MHz,  $\text{CDCl}_3$ )  $\delta$  ppm: 17.99, 21.48, 22.87, 26.60, 112.83, 117.99, 121.97, 126.09, 129.74, 134.31, 136.59, 140.21, 155.28; ESI MS :322[M+H] $^+$   $\text{C}_{20}\text{H}_{23}\text{N}_3\text{O}$ (Calcd): C, 74.74; H, 7.21; N, 13.07; O, 4.98. Obsd:C, 74.72; H, 7.22; N, 13.07; O, 4.99

4.1.2.8. 4-((2-isopropyl-5-methylphenoxy)methyl)-1-*o*-tolyl-1H-1,2,3-triazole (10). Yield 68%; white powder; M.p.: 75–76 °C; IR (ATR)  $\nu_{\text{cm}^{-1}}$ : 2956, 1502, 1456, 1411, 1383, 1287, 1247, 1166, 1093, 1030, 947, 796;  $^1\text{H}$  NMR (850 MHz,  $\text{CDCl}_3$ )  $\delta$  ppm: 1.24 (br.s., 6H, Ar—CH( $\text{CH}_3$ ) $_2$ ), 2.26 (br.s., 3H, Ar—CH $_3$ ), 2.38 (br.s., 3H, Ar—CH $_3$ ), 3.35 (br.s., 1H, Ar—CH( $\text{CH}_3$ ) $_2$ ), 5.33 (br.s., 2H, O—CH $_2$ —), 6.83 (br.s., 1H, Ar—H), 6.90 (br.s., 1H, Ar—H), 7.15 (br.s., 1H, Ar—H), 7.40 (br. s., 2H, Ar—H), 7.43 (br.s., 1H, Ar—H), 8.20 (br.s., triazole proton);  $^{13}\text{C}$  NMR (214 MHz,  $\text{CDCl}_3$ )  $\delta$  ppm: 17.93, 21.46, 22.84, 26.69, 62.32, 112.96, 122.00, 126.12, 126.94, 130.07, 131.57, 133.78, 134.32, 136.58, 155.29; ESI MS: 322[M+H] $^+$   $\text{C}_{20}\text{H}_{23}\text{N}_3\text{O}$ (Calcd): C, 74.74; H, 7.21; N, 13.07; O, 4.98. Obsd:C, 74.73; H, 7.22; N, 13.06; O, 4.99.

4.1.2.9. 4-((2-isopropyl-5-methylphenoxy)methyl)-1-(4-nitrophenyl)-1H-1,2,3-triazole (11). Yield 85%; yellow powder; M.p.: 144–145 °C; IR (ATR)  $\nu_{\text{cm}^{-1}}$ : 3055, 2962, 1610, 1597, 1523, 1506, 1456, 1405, 1334, 1256, 1238, 1166, 1096, 1039, 1019, 848;  $^1\text{H}$  NMR (850 MHz,  $\text{CDCl}_3$ )  $\delta$  ppm: 1.24 (d,  $J = 6.7$  Hz, 6H, Ar—CH( $\text{CH}_3$ ) $_2$ ), 2.37 (s, 3H, Ar—CH $_3$ ), 3.34 (m, 1H, Ar—CH( $\text{CH}_3$ ) $_2$ ), 5.34 (br.s., 2H, O—CH $_2$ —), 6.83–6.85 (m, 2H, Ar—H), 7.16 (d,  $J = 7.78$  Hz, 1H, Ar—H), 8.03 (d,  $J = 8.30$  Hz, 2H, Ar—H), 8.24 (br.s., 1H, triazole proton), 8.45 (d,  $J = 7.78$  Hz, 2H, Ar—H);  $^{13}\text{C}$  NMR (214 MHz,  $\text{CDCl}_3$ )  $\delta$  ppm: 21.42, 22.87, 26.62, 62.18, 112.72, 120.67, 122.19, 125.65, 126.21, 134.25, 136.67, 147.26, 155.09; ESI MS: 353 [M+H] $^+$   $\text{C}_{19}\text{H}_{20}\text{N}_4\text{O}_3$  (Calcd): C, 64.76; H, 5.72; N, 15.90; O, 13.62. Obsd:C, 64.74; H, 5.73; N, 15.90; O, 13.63.

4.1.2.10. 3-(4-((2-isopropyl-5-methylphenoxy)methyl)-1H-1,2,3-triazol-1-yl)benzoic acid (12). Yield 85%; white powder; M.p.: 145–146 °C; IR (ATR)  $\nu_{\text{cm}^{-1}}$ : br. peak 3000–2600, 1705, 1610, 1592, 1505, 1457, 1409, 1359, 1309, 1291, 1259, 1169, 1116, 1095, 1054, 810;  $^1\text{H}$  NMR (850 MHz,  $\text{CDCl}_3$ )  $\delta$  ppm: 1.25 (d,  $J = 5.71$  Hz, 6H, Ar—CH( $\text{CH}_3$ ) $_2$ ), 2.38 (s, 3H, Ar—CH $_3$ ), 3.33–3.37 (br.s. 1H, Ar—CH( $\text{CH}_3$ ) $_2$ ), 5.32 (s, 2H, O—CH $_2$ —), 6.84 (d,  $J = 7.78$  Hz, 1H, Ar—H), 7.16 (d,  $J = 7.27$  Hz, 1H, Ar—H), 7.73 (t,  $J = 7.01$  Hz, 1H, Ar—H), 8.19 (br.s., 1H, Ar—H), 8.25 (d,  $J = 7.27$  Hz, 1H, Ar—H), 8.54 (br.s., 1H);  $^{13}\text{C}$  NMR (850 MHz,  $\text{CDCl}_3$ )  $\delta$  ppm: 21.47, 22.86, 26.56, 62.69, 112.82, 114.10, 116.69, 121.98, 122.46, 126.66, 134.21, 136.55, 155.32, 168.90; ESI MS: 352 [M+H] $^+$   $\text{C}_{20}\text{H}_{21}\text{N}_3\text{O}_3$  (Calcd): C, 68.36; H, 6.02; N, 11.96; O, 13.66. Obsd:C, 68.33; H, 6.03; N, 11.96; O, 13.68.

4.1.2.11. 4-((2-isopropyl-5-methylphenoxy)methyl)-1-(1-(4-((2-isopropyl-5-methylphenoxy)methyl)-1H-1,2,3-triazol-1-yl)naphthalen-5-yl)-1H-1,2,3-triazole (13). Yield: 72%; M.p.: 188–189 °C; IR: 3073, 2977, 1515, 1509, 1451, 1420, 1253, 1160, 1011, 831, 807;  $^1\text{H}$  NMR (850 MHz,  $\text{CDCl}_3$ )  $\delta$  ppm: 1.24 (d,  $J = 6.75$  Hz, 6H, Ar—CH( $\text{CH}_3$ ) $_2$ ), 2.40 (s, 3H, Ar—CH $_3$ ), 3.35–3.38 (m, Ar—CH( $\text{CH}_3$ ) $_2$ ), 5.43 (br.s., 2H, O—CH $_2$ —), 6.85 (d,  $J = 7.27$  Hz, 1H, Ar—H), 6.93 (br.s., 1H, Ar—H), 7.17 (d,  $J = 7.27$  Hz, 1H, Ar—H), 7.70 (t,  $J = 7.53$  Hz, 1H, Ar—H), 7.76 (d,  $J = 6.75$  Hz, 1H, Ar—H), 7.85 (d,  $J = 7.27$  Hz, 1H, Ar—H), 8.21 (br.s., 1H, triazole proton);  $^{13}\text{C}$  NMR (214 MHz,  $\text{CDCl}_3$ )  $\delta$  ppm: 21.45, 22.87, 26.66, 62.13, 112.99, 122.15, 124.92, 126.19, 127.15, 129.54, 134.36, 136.64, 155.21; ESI MS: 587 [M+H] $^+$ .  $\text{C}_{36}\text{H}_{38}\text{N}_6\text{O}_2$  (Calcd): C, 73.69; H, 6.53; N, 14.32; O, 5.45. Obsd: C, 73.67; H, 6.54; N, 14.32; O, 5.46.

## 4.2. Biological activities

### 4.2.1. Cytotoxicity activity

The human breast tumour cell lines, MCF-7 and MDA-MB-231 and normal epithelial embryonic kidney cells HEK-293 were cultured in Dulbecco's Modified Eagle's Medium (DMEM) with 10% fetal bovine serum, 2 mM L-glutamine and 100  $\mu\text{g}/\text{mL}$  penicillin/streptomycin. Cells were maintained at 37 °C in 5%  $\text{CO}_2$  in a humidified incubator. All cells were sub-cultured 3 times/week by trypsinization using TrypLE Express (1 $\times$ ). The compounds 3–13 were evaluated for antiproliferative effect using the MTT viability assay of MCF-7, MDA-MB-231, and normal epithelial embryonic kidney cells HEK-293 to calculate the relative  $\text{IC}_{50}$  values for each compound. Cells were seeded in 96-well plates at a density of  $10 \times 10^3$  cells/mL in a total volume of 200  $\mu\text{L}$  per well. 0.1% of DMSO was used as a vehicle control. After 24 h, the cells were treated with 2  $\mu\text{L}$  test compound which had been pre-prepared as stock solutions to furnish the concentration range of study, 0.01  $\mu\text{M}$  to 100  $\mu\text{M}$ , and re-incubated for 72 h. The culture medium was then removed, and the cells washed with phosphate buffered saline (PBS) and 100  $\mu\text{L}$  MTT was added (final concentration of 5 mg/mL MTT). Cells were incubated for 4 h in darkness at 37 °C. 200  $\mu\text{L}$  DMSO was then added to each well and the cells maintained at room temperature in darkness for 20 min. Absorbance was detected with a microplate reader at 570 nm. Results were expressed as percentage viability relative to vehicle control (100%). Dose response curves were plotted and  $\text{IC}_{50}$  values were obtained using Prism software (GraphPad Software, Inc., La Jolla, CA, USA). All the experiments were repeated in three independent experiments.

### 4.2.2. In vitro thymidylate synthase enzymatic activity

The activity was performed as reported earlier.<sup>44,45</sup> It involves a mixture containing 2-mercaptoethanol (0.1 M), (6R,S)-tetrahydrofolate (0.0003 M), formaldehyde (0.012 M),  $\text{MgCl}_2$  (0.02 M), dUMP (0.001 M), TrisHCl (0.04 M), and NaEDTA (0.00075 M). This assay was done spectrophotometrically at 30 °C and pH 7.4. The reaction was initiated by the addition of an amount of enzyme giving a change in absorbance at 340 nm of 0.016/min in the absence of inhibitor. The percent inhibition was determined at a minimum of four inhibitor concentrations within 20% of the 50% point. The standard deviations for determination of the 50% points were within  $\pm 10\%$  of the values given.

### 4.2.3. Cell cycle analysis

MCF-7 cells were seeded at a density of  $1 \times 10^5$  cells/well in 6-well plates and treated with compound 10 (10  $\mu\text{M}$ ) for 48 h. After trypsinization, the cells were collected by and centrifuged at 800g for 15 min. Cells were fixed in ice-cold 70% ethanol overnight at  $-20$  °C. Fixed cells were centrifuged at 800g for 15 min and stained with 50  $\mu\text{g}/\text{mL}$  of PI, containing 50  $\mu\text{g}/\text{mL}$  of DNase-free RNase A, at 37 °C for 30 min. The DNA content of cells (10,000 cells) was analyzed by flow cytometer at 488 nm using a FACSCalibur flow cytometer (BD Biosciences, San Jose, CA, USA).

### 4.2.4. Annexin V/PI apoptotic assay

Flow cytometry using Annexin V and propidium iodide (PI) was performed to detect apoptotic cell death. MCF-7 cells were seeded in 6 well plates at density of  $1 \times 10^5$  cells/well and treated with vehicle (0.1% (v/v) EtOH), or compound 10 (10  $\mu\text{M}$ ) for 48 h. Cells were then harvested and prepared for flow cytometric analysis. Cells were washed in 1X binding buffer and incubated in the dark for 30 min on ice in Annexin V-containing binding buffer [1:100]. Then, cells were re-suspended in PI-containing binding buffer [1:1000]. Samples were analyzed immediately using the BD Accuri flow cytometer and Graph-Pad Prism software version 5.01 for analysis the data. Four populations are produced during the assay Annexin V and PI negative (Q4, healthy cells), Annexin V positive and PI negative (Q3, early apoptosis), Annexin V and PI positive (Q2, late apoptosis) and Annexin V negative and PI

positive (Q1, necrosis).

#### 4.3. Computational details and molecular docking

##### 4.3.1. Ligand preparation

The DFT Calculations have been performed foremostly using the Jaguar.<sup>39,40</sup> DFT simulations have been utilized for geometrical optimizations of studied structures, employing the B3LYP exchange–correlation functional<sup>41</sup> and MIDIX basis set.<sup>42</sup> The chemical reactivities were calculated at DFT with B3LYP and 6-311++G\*\* basis set used for the simulations frontier molecular orbital and molecular electrostatic maps. The optimized geometry for the tested compounds were used for generate all possible states, such as tautomeric and stereo-isomeric followed by minimization at the OPLS force field.<sup>46</sup>

##### 4.3.2. Protein formulation and active site prediction:

3D crystal structure of TM protein (PDB ID: 6QXG<sup>47</sup>) was obtained from the Protein Data Bank. Charges with bond orders were assigned, H atoms were added to heavy atoms. Then, selenomethionines and selenocysteines transferred to methionines and cysteines. All water molecules were removed. The OPLS force field used for protein minimization to set a maximum heavy atom 0.30 Å RMSD. The binding pockets of protein have been identified using the CASTp package,<sup>48</sup> which applies the modern algorithmic and geometrical analysis for analyzing and validation of the binding pockets.

##### 4.3.3. Receptor grid generation and molecular docking

The Glide software<sup>49</sup> was utilized for generation of receptor grid and docking simulation process. The created grid was parameterized using default software parameter (1.00 van der Waals, 0.25 cut-off of charge), and submitted to OPLS force field. Then produced and centroid the definite cubic box (12 Å × 12 Å × 12 Å) into active site. This box was used for docking study which were carried out using extra precision and write XP descriptor information. This generates favourable ligand poses which are further screened through filters to examine spatial fit of the ligand in the active site. Ligand poses which pass through initial screening are subjected to evaluation and minimization of grid approximation. Scoring was then carried on energy minimized poses to generate Glide score

#### Declaration of Competing Interest

The authors declare that they have no known competing financial interests or personal relationships that could have appeared to influence the work reported in this paper.

#### Acknowledgements

A.S.A.A acknowledges Taif University Researchers Supporting Project (Number TURSP-2020/44) for financial assistance. M.M.A and S.N. thanks Chemistry department, Albaha university for providing the necessary facilities to carry out the project work. We also thank Ms. Safaa S. Bayashut, King Abdulaziz University for helping in performing the pharmacological activities.

#### Appendix A. Supplementary material

Supplementary data to this article can be found online at <https://doi.org/10.1016/j.bmc.2021.116136>.

#### References

- Unnati S, Ripal S, Sanjeev A, Niyati A. *Chin J Nat Med*. 2013;11:0016–0023.
- Khalid EB, Ayman EE, Rahman H, Abdelkarim G, Najda A. *Tumor Biol*. 2016;37:14513–14536.
- Gordaliza M. *Clin Transl Oncol*. 2007;9:767–776.
- Utsugi T, Shibata J, Sugimoto Y, et al. *Cancer Res*. 1996;56:2809–2814.
- Hartmann JT, Lipp HP. *Drug Saf*. 2006;29:209–230.
- Butler MS, Robertson AAB, Cooper MA. *Nat Prod Rep*. 2014;31:1612–1661.
- Khalifa ME, Gobouri AA, Kabli FM, Altalhi TA, Almalki ASA, Elemshaty AM. *J Het Chem*. 2019;56:1426–1436.
- Fleming RA, Miller AA, Steward CF. *Clin Pharm*. 1989;8:274–293.
- Hait WN, Rubin E, Alli E, Goodin S. *Update Cancer Therapeu*. 2007;2:1–18.
- Malonne H, Atassi G. *Anticancer Drugs*. 1997;8:811–822.
- Cersisimo RJ. *Ann Pharmacother*. 1998;32:1324–1333.
- Erllichman C, Sargent DJ, Engl N. *J Med*. 2004;351:391–392.
- Dubois J. *Exp Opin Ther Patents*. 2006;16:1481–1496.
- Xiao Z, Morris-Natschke SL, Lee KH. *Med Res Rev*. 2016;36:32–91.
- Saklani A, Kutty SK. *Drug Discov Today*. 2008;13:161–171.
- Liu W, Zhai Y, Heng X, et al. *J Drug Target*. 2016;24:694–702.
- Seca AML, Diana CGA. *Int J Mol Sci*. 2018;19:263–272.
- Dheer JD, Singh D, Kumar G, et al. *Curr Bioact Compd*. 2019;15:454–474.
- Javan AJ, Javan MJ. *Food Chem*. 2014;165:451–459.
- Nesterkina M, Kravchenko I. *I Pharmaceuticals (Basel)*. 2017;10:47–55.
- Cui Z, Li X, Nishida Y. *Lett Drug Des Discov*. 2014;11:877–885.
- Kurt BZ, Gazioglu I, Dag A, et al. *Bioorg Med Chem*. 2017;25:1352–1363.
- Diab-Asaf M, Semaan J, El-Sabban M, et al. *Anticancer Agents Med Chem*. 2018;18:1–6.
- Islam MT, Khalipha ABR, Bagchi R, et al. *IUBMB Life*. 2019;71:9–19.
- Balabadre S, Kotni MK, Manga V, Allanki AD, Prasad R, Sijwal PS. *Bioorg Med Chem*. 2017;25:221–232.
- Pathak PS, Bakale RD, Kulkarni RS, et al. *Bioorg Med Chem*. 2020;30:1275789.
- Bozorov K, Zhao J, Aisa HA. *Bioorg Med Chem*. 2019;27:16.
- Lu GQ, Li XY, Mohamed OK, Wang D, Meng FH. *Eur J Med Chem*. 2019;171:282–296.
- Baraniak D, Baranowski D, Ruszkowski P, Boryski J. *Nucleosides Nucleotides Nucleic Acids*. 2019;38:807–835.
- Alam MM, Almalki ASA, Neamatallah T, Ali NM, Malebari AM, Nazreen S. *Pharmaceuticals*. 2020;13:390–405.
- Rode W, Les A. *Acta Biochim Pol*. 1996;43:133–142.
- Oughton JAH, Tillman DM, Harwood FG. *Clin Cancer Res*. 1995;1(7):723–730.
- Alghamdi AA, Alam MM, Nazreen S. *Turk J Chem*. 2020;44:1068–1084.
- <http://www.swissadme.ch>.
- Lipinski CA, Lombardo F, Dominy BW, Freener PJ. *Adv Drug Del Rev*. 2001;46:3–26.
- Williams GH, Stoerber K. *J Pathol*. 2012;226:352–364.
- Xu W, Jing L, Wang Q, et al. *Oncotarget*. 2015;6:30017–30034.
- Alzhrani ZMM, Alam MM, Neamatallah T, Nazreen S. *J Enzyme Inhib Med Chem*. 2020;35:1116–1123.
- Bochevarov AD, Harder E, Hughes TF, et al. *Int J Quantum Chem*. 2013;113:2110–2142.
- Jacobson LD, Bochevarov AD, Watson MA, et al. *J Chem Theory Comput*. 2017;13:5780–5797.
- Van Ha N, Dat DT, Nguyet TT. *VNU J Sci Nat Sci Technol*. 2019;35(4):55–62.
- Easton RE, Giesen DJ, Welch A, Cramer CJ, Truhlar DG. *Theor Chim Acta*. 1996;93:281–301.
- War JA, Jalaja K, Mary YS, et al. *J Mol Struct*. 2017;1129:72–85.
- Wahba AJ, Friedkin M. *J Biol Chem*. 1962;237:3794–3801.
- Davison VJ, Sirawaraporn W, Santi DV. *J Biol Chem*. 1989;264:9145–9148.
- Siu SWL, Pluhackova K, Bockmann RA. *J Chem Theory Comput*. 2012;8:1459–1470.
- Pozzi C, Ferrari S, Luciani R, Tassone G, Costi MP, Mangani S. *Molecules*. 2019;24:1257–1271.
- Tian W, Chen C, Lei X, Zhao J, Liang J. *Nucleic Acids Res*. 2018;46:W363–W367.
- Friesner RA, Banks JL, Murphy RB, et al. *J Med Chem*. 2004;47:1739–1749.